Electronic Supplementary Material (ESI) for Nanoscale.

Supplementary Information

for

Using Cyclocarbon Additive as Cyclone Separator to Achieve Fast Lithiation and Delithiation Without Dendrite Growth in Lithium-ion Batteries

Jiacheng Gong, *Jiabao Zhu*, *Xiao He* * and *Jinrong Yang* *

Table of Contents

Section 1. Lithium-ion batteries

Note S1. The calculated details of adsorption energies and cell voltages.

The overall reaction of $Li^+/Li@C$ (C refers to carbon-based materials) is simplified and expressed by the following expression:

$$Li^+ + Li@C \leftrightarrow Li + Li^+@C$$

The cell voltage can be determined by the Nernst equation[1, 2]:

$$V_{cell} = -\Delta G_{cell} / zF$$

where z is +1 a.u., on behalf of the charge of the Li^+, F is the Faraday constant, generally regarded as 96500 C/mol, and ΔG_{cell} is Gibbs free energy. ΔG_{cell} can be calculated by

$$\Delta G_{cell} = \Delta E_{react} + P\Delta V_{react} - T\Delta S_{react}$$

where ΔE_{react} is the reaction energy, P is the intensity of pressure, ΔV_{react} is the volume change, T is the temperature, and ΔS_{react} is the entropy change. Since the contributions of entropy ($T\Delta S_{react}$) and volume ($P\Delta V_{react}$) effects to the cell voltage are extremely small[3] for condensed matter reaction at 0 K, ΔG_{cell} of the chemical reaction of Li^+ cation cell can be approximated as the internal energy, calculated by

$$\Delta G_{cell} = \Delta E_{react} = \Delta E_{tot} = E_{Li} + E_{Li^+@C} - E_{Li@C} - E_{Li^+}$$

The internal energy ΔE_{tot} can be seen as the adsorption energy of Li^+ ions minus the adsorption energy of Li atoms ($\Delta E_{tot} = E_{adsLi^+} - E_{adsLi}$), which means that the V_{cell} is at rest with both Li^+ ion and Li atom adsorptions. The E_{ads} and V_{cell} of $Na^+/Na@C$ and $K^+/K@C$ can also be calculated in the same way as $Li^+/Li@C$.

Note S2. The calculated details of strain energies and Julg structure index.

The strain energy can be calculated by

$$E_{Li^+/Li} = E_{aft} - E_{bef}$$

where E_{aft} and E_{bef} are the energy of C_{14} after interacting with Li^+/Li and before adsorption.

The Julg structure index is defined as[4]

$$A_{jLi^+/Li} = 1 - (225/n) \sum(1 - R_r/R)^2$$

where n is the number of carbon atoms, and it is 14 for C_{14}. R_r is the length of each C-C bond on the ring, and R is the average C-C bond length. When every R_r is equal to R, the $A_{jLi^+/Li}$ is going to be zero meaning absolutely aromatic.

Note S3. The optimization details of periodical geometries.

We use the VASP code[5-8] to optimize the periodical geometries of C_{14}@C_{14}, C_{14}@Graphene, Li@C_{14}, Li@Graphene and Li@C_{14}-Graphene. The generalized gradient approximation (GGA)[9] with the Perdew-Burke-Ernzerhof (PBE)[10] functional is employed to describe the electron exchange-correlation interactions. DFT-D3 method of Grimme with zero-damping function[11] is used to describe weak interaction of adsorption, and the cut-off energy is set to 400 eV for all calculations. The integration of the Brillouin zone is conducted using a 3 × 3 × 1 k-points mesh. The vacuum space of 20 Å is set in the direction normal to the sheets to avoid interactions between periodic images. For geometrical optimization, the graphene base is fixed, but C_{14} and Li are relaxed in every direction. Convergence in energy and force are set at 1×10^{-4} eV/atom and 0.02 eV/Å, respectively.

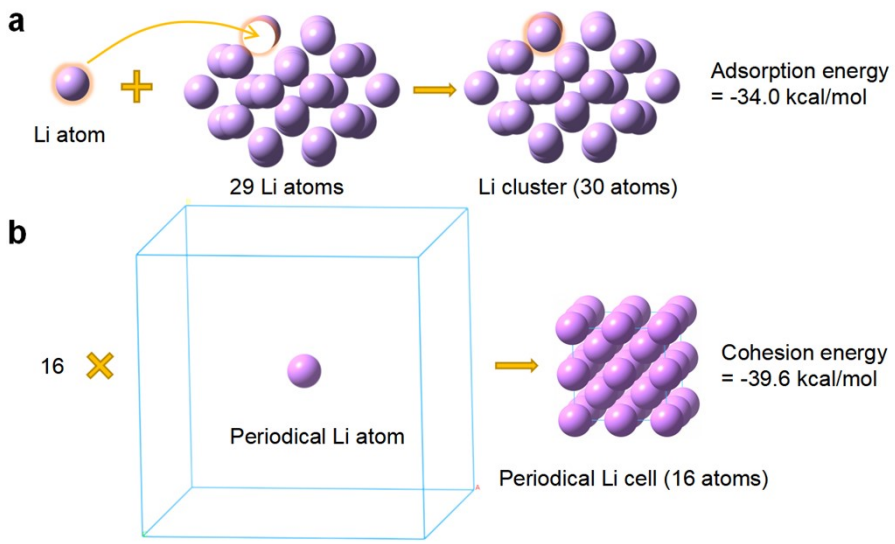

Figure S1. **The adsorption energy and cohesion energy of Li atoms.**

(a), The adsorption energy of the Li atom interacting with other Li atoms in a cluster consisting of 30 Li atoms. The geometries are optimized by the density functional theory, at the level of ωB97XD/6-311G(d). **(b)**, The cohesion energy of a Li atom. The periodical geometries of the Li cell and sole Li atom are optimized by VASP, using the DFT-D3 corrected GGA-PBE method. The cohesion energy is required to assemble an amount of a substance from the point where intermolecular forces dissolve to the point where a complete complex is formed, as a measure of how tightly the molecules of a substance are bound together. The cohesion of a Li atom in a periodical cell (-34.0 kcal/mol), close to the adsorption of a Li atom in a cluster (-43.5 kcal/mol), is stronger than the adsorption between a Li atom and graphene (-20.5 kcal/mol) or carbon nanotube (-36.4 kcal/mol) in Fig. 1a.

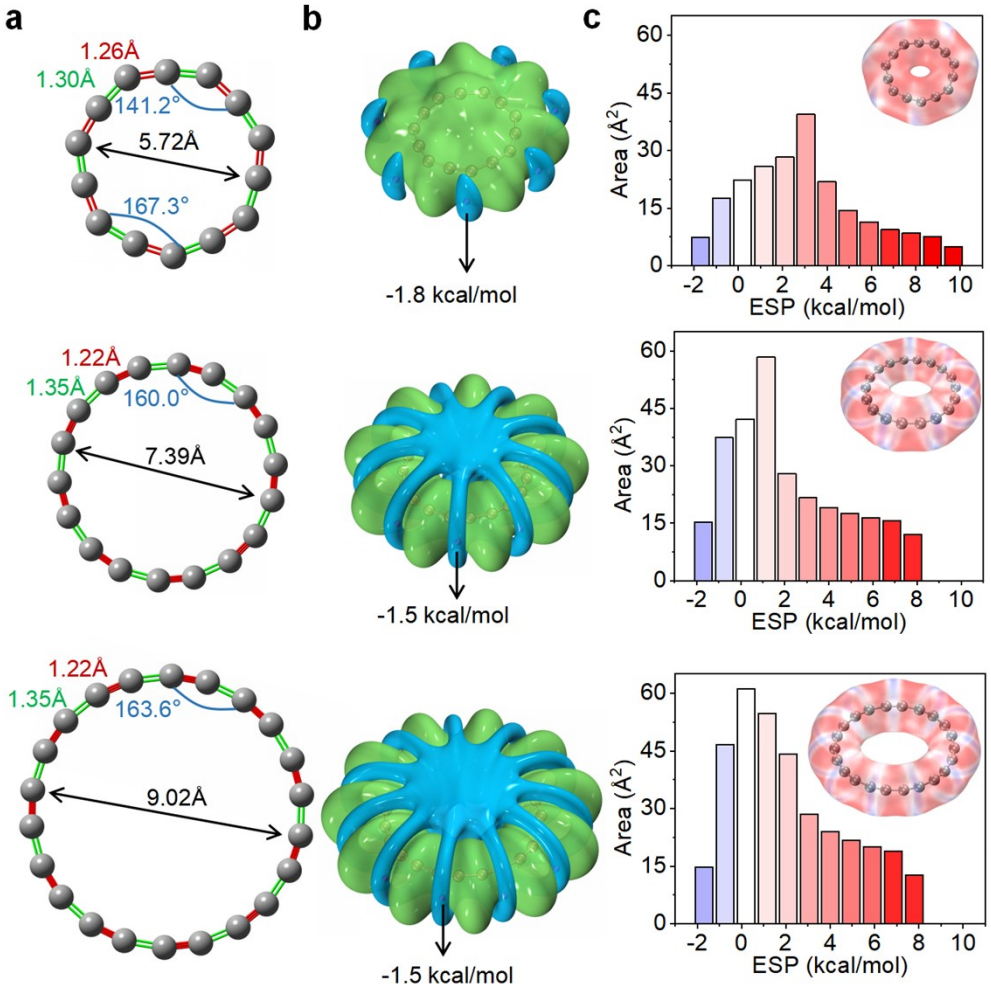

Figure S2. Static analysis of C_{14}, C_{18} and C_{22}.

(a), Geometries of C_{14} (Top), C_{18} (Middle) and C_{22} (Bottom). The gray spheres are carbon atoms. The red bonds represent the shorter C-C bonds, and their average length is 1.26 Å for C_{14} and 1.22 Å for C_{18} and C_{22}. The green bonds denote the longer C-C bonds, and their average length is 1.30 Å for C_{14} and 1.35 Å for C_{18} and C_{22}. The blue arcs are bond angles between adjacent short and long C-C bonds. For C_{14}, its alternative angles are 141.2° and 167.3°, respectively. And there is no evident difference of alternation among angles in C_{18} and C_{22}, which are 160.0° and 163.6°. The black double-headed arrows represent the diameter of C_{14}, C_{18} and C_{22} rings, which are 5.72 Å, 7.39 Å and 9.02 Å, respectively. All geometries are optimized by Gaussian at the level of ωB97XD/6-311+G(2d). **(b)**, Isosurface maps of the electrostatic potential (ESP) of C_{14} (Top), C_{18} (Middle) and C_{22} (Bottom). Positive isosurfaces are in green, and negative ones are in blue. To ensure the integrity of isosurfaces, both of their isovalues are set as 0.0014 a.u., 0.0080 a.u. and 0.0070 a.u. for C_{14}, C_{18} and C_{22} rings, respectively. The purple spheres inside the blue isosurface denote the minimum point of negative ESP, which is -1.8 kcal/mol in C_{14} and -1.5 kcal/mol in C_{18} and C_{22}. **(c)**, Area distribution of different ESP intervals on the vdW surface of C_{14} (Top), C_{18} (Middle) and C_{22} (Bottom). All isovalues of vdW isosurface are 0.001 a.u.. The brighter the red, the larger the positive value of ESP and the more solid the blue, the smaller the negative value of ESP. In C_{14}, ESP on the vdW surface is distributed from -1.6 kcal/mol to 9.8 kcal/mol. That value is between -1.5 kcal/mol to 8.0 kcal/mol on the surface of C_{18} and between -1.4 kcal/mol to 8.0 kcal/mol on that of C_{22}.

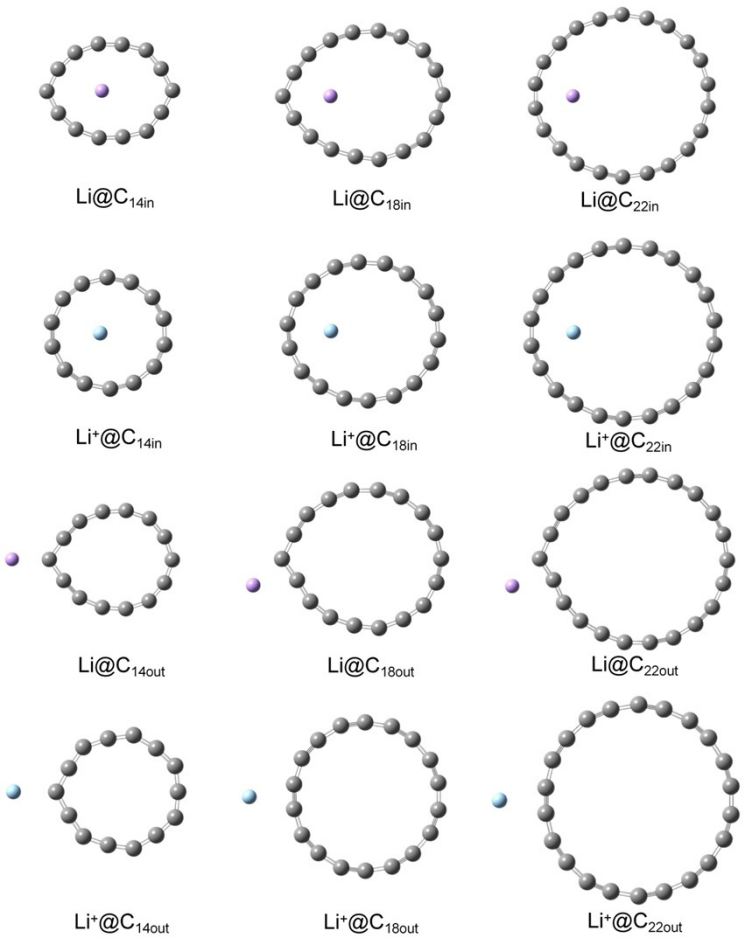

Figure S3. Top view of geometries of Li^+/Li combined inside and outside C_{14}, C_{18} and C_{22}.

All geometries are optimized by Gaussian at the level of ωB97XD/6-311+G(2d). The distortion of cyclocarbons that interacting with Li is larger than that with Li^+ (refer to Table S3).

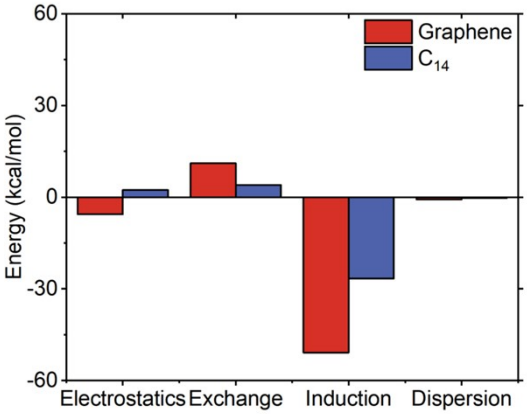

Figure S4. Components of the interaction energy between Li^+ ion and C_{14} or Graphene.

The symmetry-adapted perturbation theory (SAPT) analysis at sSAPT0/jun-cc-pVDZ level was carried out by PSI4 1.3.2 code[12]. The ion-π interaction of graphene is stronger than that of C_{14} since the induction energy between the Li^+ ion and graphene is -50.8 kcal/mol, far lower than that between the Li^+ ion and C_{14} (-26.6 kcal/mol). And the electrostatic energy between the Li^+ ion and graphene is calculated to be -5.6 kcal/mol, indicating a favorable mutual interaction. In contrast, the electrostatic energy between the Li^+ ion and C_{14} is positive, measuring 2.3 kcal/mol, which hinders their combination.

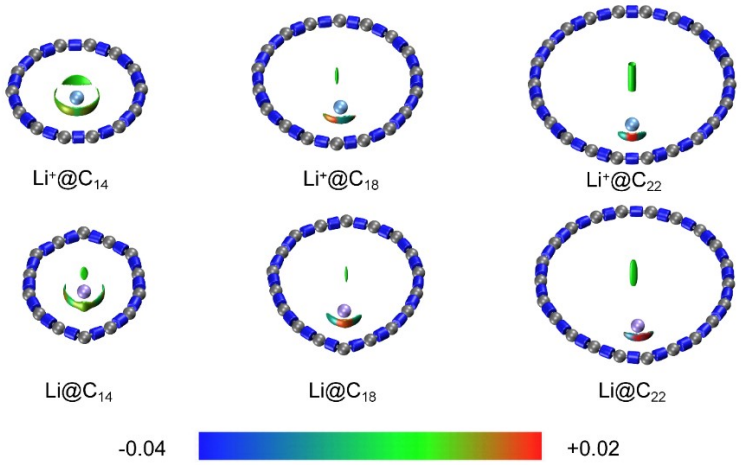

Figure S5. The interaction region indicator (IRI) maps of Li^+/Li interacted with C_{14}, C_{18} and C_{22}.

The relevant sign (λ2)ρ function can be visualized on IRI isosurfaces using different colors. In this representation, the blue region indicates a notable attraction, similar to H-bond and halogen-bond interactions. The green region represents a very weak interatomic van der Waals (vdW) interaction, while the red region signifies notable repulsion, such as steric effects within the ring and cage structures. Notably, there is a weak interaction observed in the green region between cyclocarbons and Li^+/Li, and the size of the isosurface coincides with the trend of adsorption energy (refer to Table S2). As the size of the ring increases, the size of the isosurface shrinks, and while the attraction becomes stronger, indicated by a more solid blue color, the adverse repulsion becomes more pronounced, represented by a more intense red color.

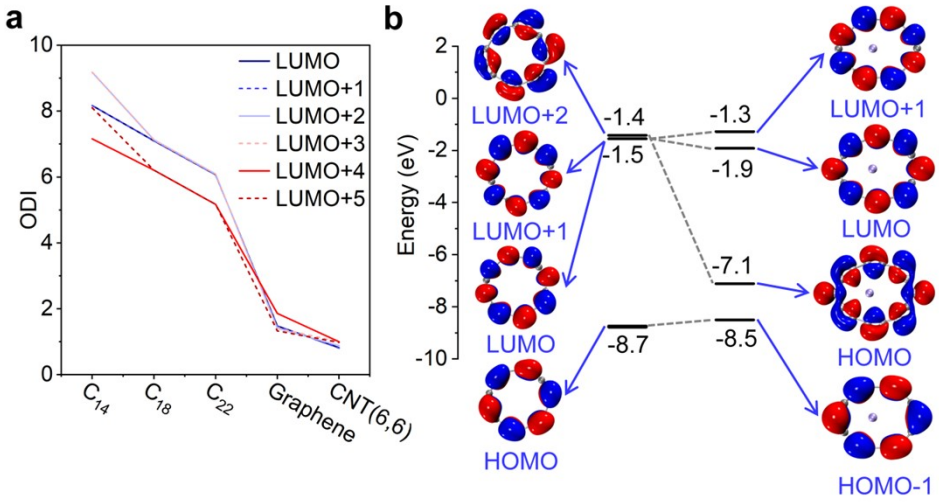

Figure S6. **The orbital analysis of C_{14}, C_{18}, C_{22}, Graphene, CNT and Li@C_{14}.**

(a), The orbital delocalization index (ODI) of LUMO, LUMO+1, LUMO+2, LUMO+3, LUMO+4 and LUMO+5 for C_{14}, C_{18}, C_{22}, graphene and CNT. For all cyclocarbons, the LUMO and LUMO+1 orbitals are out-plane π orbitals, while the LUMO+2 and LUMO+3 orbitals are in-plane π orbitals, the unique characteristic which is not found in Grap and CNT. In the case of C_{14}, the in-plane π orbitals have the largest ODI value of 9.2, indicating that LUMO+2 and LUMO+3 in C_{14} exhibit the highest electron concentration and the strongest electron adsorption compared to its out-of-plane π orbitals, with an ODI of 8.2, and the LUMO+4 orbital in Grap and CNT, with ODI of 1.9 and 1.0 each. **(b)**, Frontier molecular orbitals of C_{14} and Li@C_{14}. The LUMO+2 orbital in C_{14} adopts a similar shape to the in-plane π orbital. Red and blue regions (isovalue = 0.025 a.u.) denote the positive and negative orbital phases, respectively. This similarity is also observed in the HOMO orbital of the Li@C_{14} complex, indicating that the valence shell electron of Li is transferred to the unoccupied LUMO+2 orbital of the C_{14} ring, resulting in the formation of the occupied HOMO orbital of the complex. This electron transfer leads to a decrease in energy from -1.4 eV to -7.1 eV. Furthermore, the HOMO orbital in C_{14} becomes the HOMO-1 orbital in Li@C_{14}, while there are no changes observed in the LUMO and LUMO+1 orbitals after interaction with Li.

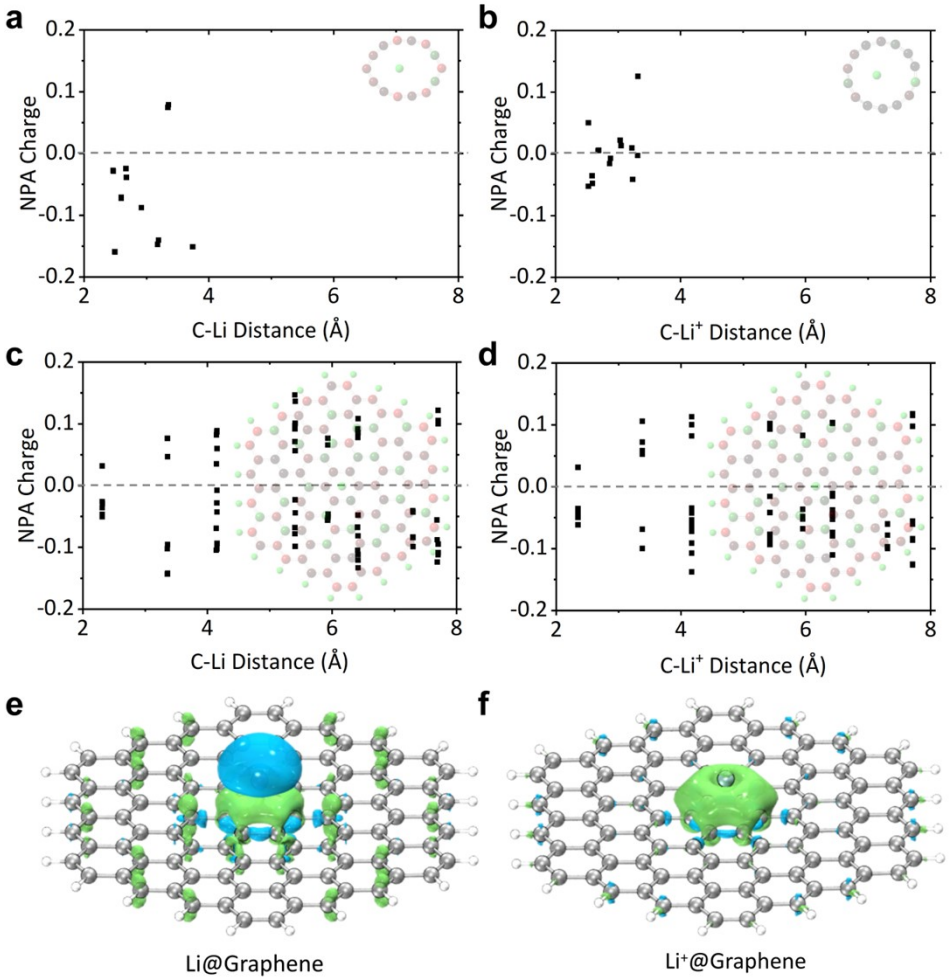

Figure S7. The charge analysis of Li/Li^+@C_{14} and Li/Li^+@Graphene.

(a), The natural population analysis (NPA) charge of C atoms in Li@C_{14}. The NPA charge of the Li atom is 0.967, indicating that it gives its valence electron to C_{14} and then turns into a positive Li^+ cation. Most of the C atoms, close to the positive Li^+ cation, present negative charges to generate a strong electrostatic attraction with the Li^+ cation. And the most negative value of NPA charge is -0.16 on the C atom, which is only 2.49 Å far from the Li^+ cation. **(b)**, The NPA charge of C atoms in Li^+@C_{14}. The NPA charge of the Li^+ ion is 0.968, indicating that there is no evident charge transfer between C_{14} and Li^+ ion, conforming to the presence of ion-π interaction. The electrostatic attraction between the Li^+ ion and C_{14} is weaker compared to that between the Li atom and C_{14} because approximately half of the C atoms exhibit negative charges around -0.05, far higher than that in Li@C_{14}. And other C atoms show positive charge, further enhancing mutual electrostatic exclusion to Li^+ ion. **(c)**, The NPA charge of C atoms in Li@Graphene. The NPA charge of the Li atom is 0.951, indicating that it turns into a Li^+ cation with a positive charge. Although there is a similar amount of charge transfer from the Li atom to the C atoms in Li@Graphene compared to Li@C_{14}, the negative charges in Li@Graphene are dispersed by the presence of numerous C atoms with delocalized π orbitals. Consequently, the electrostatic attraction in Li@Graphene is weaker than that in Li@C_{14}, primarily attributed to the slightly higher negative charge (-0.05) of the C atoms closest to the Li atom in graphene. **(d)**, The NPA charge of C atoms in Li^+@Graphene. The NPA charge of the Li^+ ion is determined to be 0.951, indicating a similar ion-π interaction between Li^+ and graphene as that in Li^+@C_{14}. **(e)**, The electron density difference (EDD) map of Li@Graphene.

Green and blue isosurfaces (isovalue = 0.0015 a.u.) represent the regions where the electron density is increased and decreased, respectively, after complexation between the Li atom and graphene. Electron transfer occurs from the Li atom, depicted by the blue isosurface, to the π orbitals of the nearest carbon atoms in graphene, represented by the green isosurface. And the remaining carbon atoms disperse the acquired electrons, verified by scattered green isosurfaces within the carbon atoms. This observation confirms that the dispersed negative charge results in a weaker electrostatic attraction compared to $Li@C_{14}$. **(f)**, The EDD map of Li^+@Graphene. There is no electron transfer between Li^+ and graphene, the same as in $Li^+@C_{14}$.

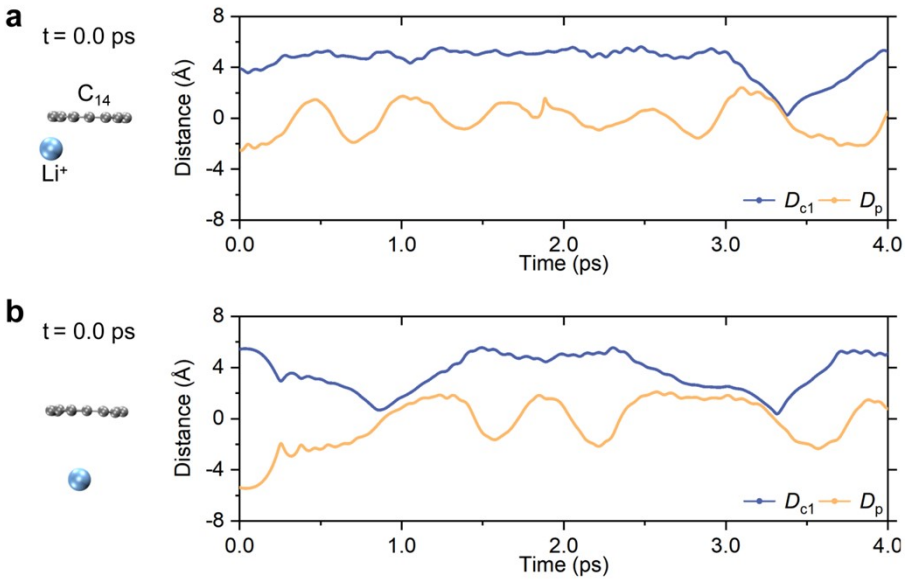

Figure S8. 4.0 ps trajectory of *ab initio* molecular dynamics simulations of outside Li^+ ion, at different locations, across C_{14} at 300.00K, described by D_p (Blue) and D_{c1} (Yellow).

The level of ωB97XD/def-TZVP is adopted for *ab initio* molecular dynamics simulation. D_{c1} is the distance between the Li^+ ion or Li atom and the mass center. And D_p is the shortest perpendicular distance from the Li^+ ion or Li atom to the plane of C_{14}. **(a)**, The dynamical course of outside Li^+ positioned 3.9 Å away from the center of C_{14} and -2.5 Å away from its plane initially. At 3.4 ps, both the D_p and D_{c1} values approach 0.0 Å, indicating that the Li^+ ion has completely entered the C_{14} ring. Subsequently, these values deviate from 0.0 Å, indicating that the Li^+ ion can freely move out of the ring. **(b)**, The dynamical course of outside Li^+ positioned 5.4 Å away from the center of C_{14} and -5.4 Å away from its plane initially. At 0.9 ps and 3.3 ps, both the D_p and D_{c1} values approach 0.0 Å, indicating that the Li^+ ion can entirely enter into and leave the C_{14} ring twice within a duration of 4.0 ps.

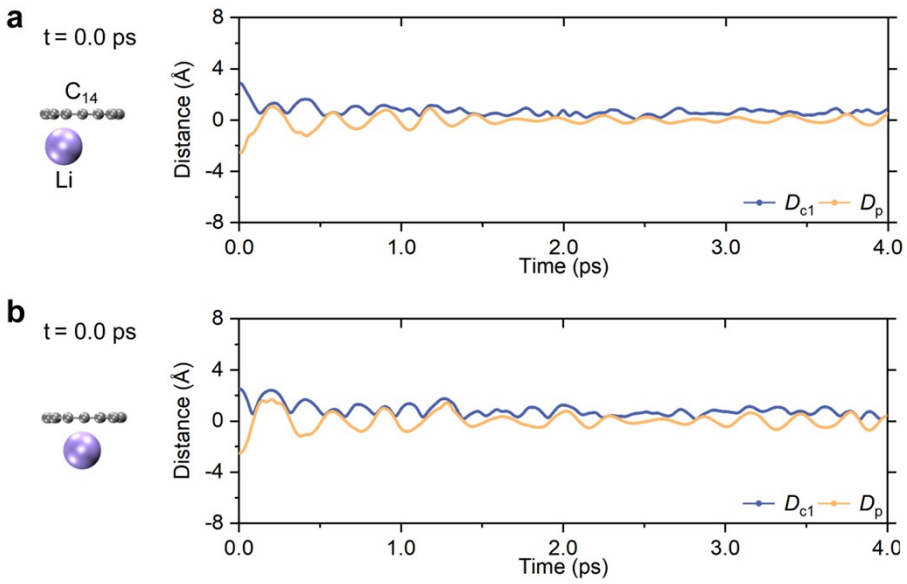

Figure S9. 4.0 ps trajectory of *ab initio* molecular dynamics simulations of outside Li atom, at different locations, adsorbed by C_{18} at 300.00K, described by D_p (Blue) and D_{c1} (Yellow).

The level of ωB97XD/def-TZVP is adopted for *ab initio* molecular dynamics simulation. D_{c1} is the distance between the Li^+ ion or the Li atom and the mass center. And D_p is the shortest perpendicular distance from the Li^+ ion or the Li atom to the plane of C_{14}. **(a)**, The dynamical course of the Li atom located 2.8 Å away from the center of C_{14} and -2.5 Å away from its plane. At 0.1 ps, both D_p and D_{c1} values approach 0.0 Å, indicating that the Li atom entirely enters the C_{14} ring. Subsequently, these values fluctuate around 0.0 Å, suggesting that Li moves up and down within a limited area but cannot entirely escape the influence of C_{14}. **(b)**, The dynamical course of the Li atom located 2.5 Å away from the center of C_{14} and -2.5 Å away from its plane. At 0.1 ps, both D_p and D_{c1} values are close to 0.0 Å, indicating that the Li atom is entirely captured inside the C_{14} ring. Subsequently, these values fluctuate around this value, suggesting that the Li atom moves up and down within the ring.

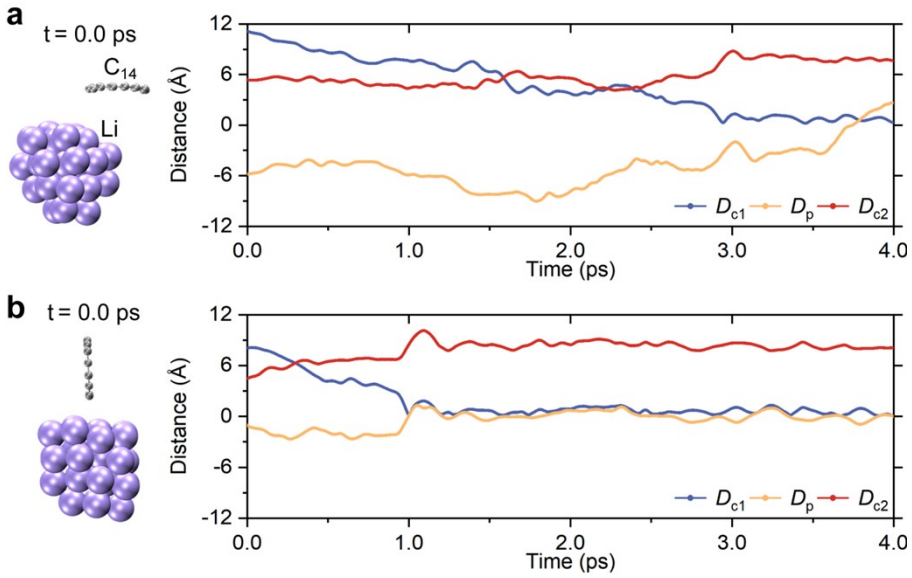

Figure S10. 4.0 ps trajectory of *ab initio* molecular dynamics simulations of outside Li in a cluster at different locations, adsorbed by C_{14} at 300K, described by D_p (Blue), D_{c1} (Yellow) and D_{c2} (Red).

The level of ωB97XD/def-TZVP is adopted for *ab initio* molecular dynamics simulation. D_{c1} is the distance between the Li^+ ion or the Li atom and the mass center. D_p is the shortest perpendicular distance from the Li^+ ion or the Li atom to the plane of C_{14}. And D_{c2} is the distance between the separated Li atom and the geometric center of the remaining Li clusters. **(a)**, The dynamical course of the Li atom, in the cluster, located at 11.0 Å from the center of C_{14} and -5.8 Å from its plane. At 2.9 ps, the values of D_p and D_{c1} are both close to 0.0 Å, indicating that the Li atom has entirely entered into the C_{14} ring. Additionally, D_{c2} experiences a slight rise from 5.3 Å to 6.5 Å, revealing that the Li atom is separated from the cluster. Subsequently, the values of D_p and D_{c1} remain around 0.0 Å, suggesting that the Li atom moves up and down within a limited area but remains influenced by the presence of C_{14} and does not entirely escape from it. **(b)**, The dynamical course of the Li atom in the cluster, located at 8.0 Å from the center of C_{14} and -1.0 Å from its plane. At 1.0 ps, both D_p and D_{c1} values are close to 0.0 Å, and the D_{c2} value increases by approximately 4.0 Å, suggesting that the Li atom becomes separated from the cluster and is captured into the C_{14} ring.

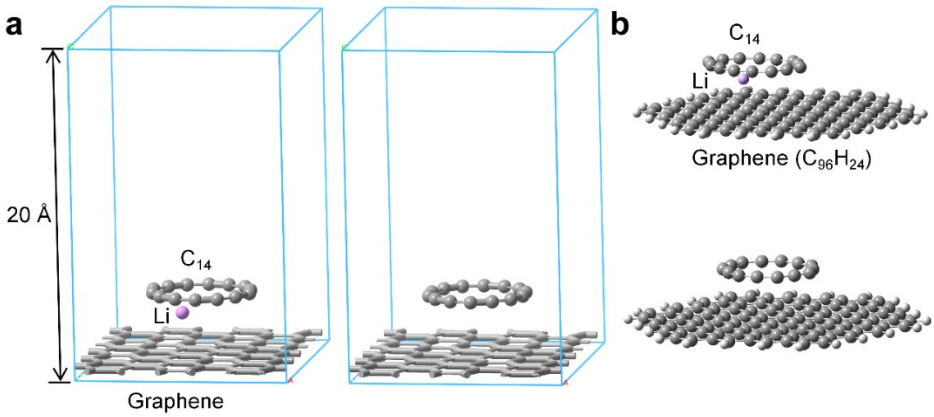

Figure S11. **The geometries of Li@C_{14}-Graphene and C_{14}@Graphene.**

(a), The periodical geometries of Li@C_{14}-Graphene and C_{14}@Graphene. The periodical geometries of a Li atom interacting with C_{14} and graphene, and C_{14} adsorbed by graphene base are optimized by VASP, using the DFT-D3 corrected GGA-PBE method. The shortest perpendicular distance from the Li atom to C_{14} is 0.7 Å, and that from the C_{14} to graphene both are around 3.1 Å. **(b)**, The geometries of Li@C_{14}-Graphene and C_{14}@Graphene, using the density functional theory. The geometries of a Li atom interacting with C_{14} and graphene, and C_{14} adsorbed by graphene base are optimized at the level of ωB97XD/6-311G(d). There are similarities between the values of the shortest perpendicular distance from the Li atom to C_{14} (0.9 Å) as well as that from the C_{14} to graphene (3.2 Å) in density functional theory and those values in periodical geometries. All the adsorption energies are exhibited in Supplementary Table S4.

Table S1. The adsorption energy of Li^+/Li combined with conventional carbon-based materials in previous research.

Carbon-based materials	E_{adsLi^+} (kcal/mol)	E_{adsLi} (kcal/mol)	Reference
CNT-(7,0)	-38.3	-20.1	
CNT-(10,0)	-49.8	-28.1	[13]
CNT-(12,0)	-48.9	-30.9	
CNT-(6,6)	-55.5	-28.1	[14]
Graphene-$C_{96}H_{26}$	-56.0	-	[15]
Graphene-$C_{96}H_{26}$	-55.8	-	[16]
Graphene-4×4	-60.2	-	[17]
Graphene-$C_{24}H_{12}$	-	-6.2	
Graphene-$C_{54}H_{18}$	-	-12.5	[18]
Graphene-$C_{92}H_{24}$	-	-18.9	
Graphene-4×4	-	-28.1	[19]
Graphene-4×4	-	-31.4	[20]
Graphene-3×3		-31.4	[21]

Table S2. The adsorption energy of Li^+/Li combined inside and outside C_{14}, C_{18} and C_{22}.

Cyclocarbon	Li^+		Li	
	E_{adsin} (kcal/mol)	E_{adsout} (kcal/mol)	E_{adsin} (kcal/mol)	E_{adsout} (kcal/mol)
C_{14}	-28.7	-27.6	-51.9	-39.7
C_{18}	-28.3	-24.6	-43.3	-38.7
C_{22}	-28.8	-25.5	-40.4	-37.6

Table S3. The length of the longest axis (*d*) and deform degree (*D*) for cyclocarbons interacted with Li^+/Li.

Cyclocarbon	*d* (Å)		*D* (%)	
	Li^+	Li	Li^+	Li
C_{14}	5.84	6.66	2.18	16.47
C_{18}	7.70	8.33	0.83	8.61
C_{22}	9.33	9.57	0.78	7.59

*The deform degree can be calculated as $D(\%) = (d_{Li^+/Li@Cn} - d_{Cn}) / d_{Cn} \times 100$, Where $d_{Li^+/Li@Cn}$ and d_{Cn} are the lengths of the longest axis of cyclocarbons after and before Li^+/Li adsorption, respectively. The original lengths d_{C14}, d_{C18} and d_{C22} are 5.72 Å, 7.39 Å and 9.02 Å before adsorption.

Table S4. The adsorption energy of C_{14} or Li interacting with graphene or C_{14} calculated by PBE and ωb97xd methods.

Base Material	E_{adsC14} (kcal mol)		E_{adsLi} (kcal/mol)	
	PBE	ωb97xd	PBE	ωb97xd
Graphene	-16.7	-10.1	-31.0	-8.5
C_{14}	-5.7	-3.7	-42.5	-51.9

Section S2. Sodium-ion batteries and potassium-ion batteries

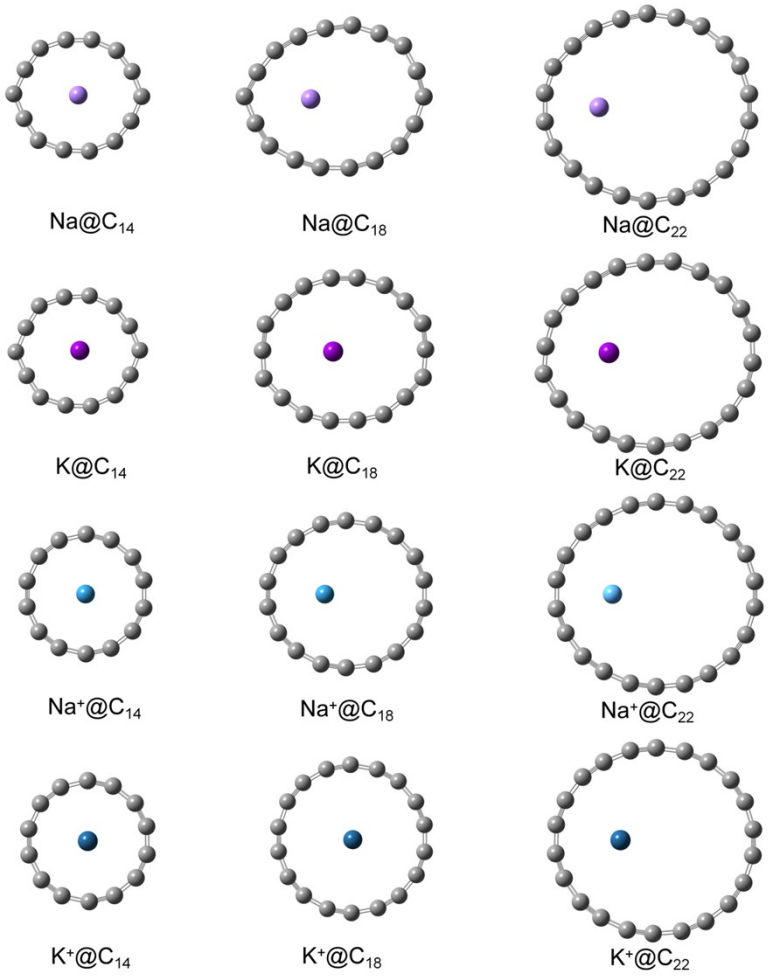

Figure S12. Top view of geometries for Na/K, Na^+/K^+ combined inside C_{14}, C_{18} and C_{22}.

All geometries are optimized by Gaussian at the level of ωB97XD/6-311+G(2d). The distortion of cyclocarbons interacted with Na/K is larger than that with Na^+/K^+ (refer to Table S11 and Table S12)

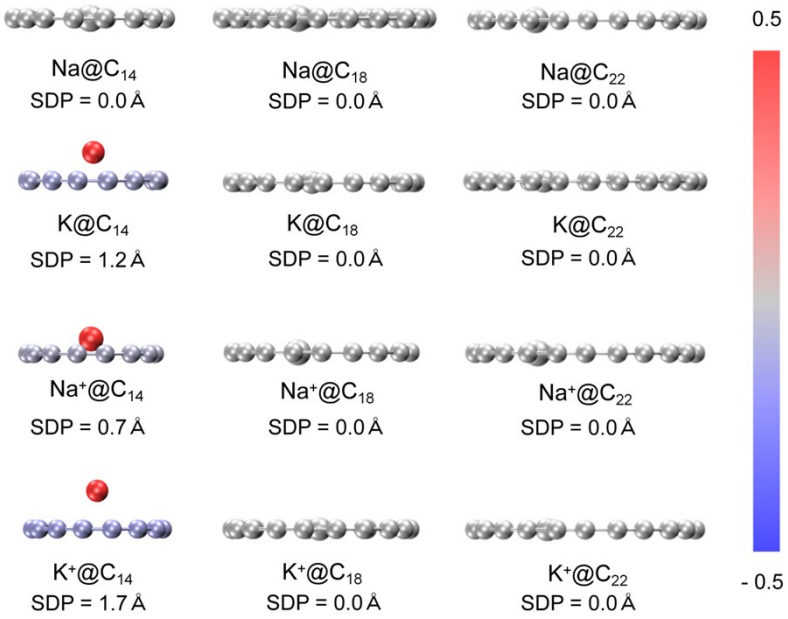

Figure S13. Side view of geometries and the span of deviation from plane (SDP) for Na^+/Na, K^+/K combined inside C_{14}, C_{18} and C_{22}.

Atoms and ions are colored in different colors based on their d^s values—the more solid the red, the more positive the value. SDP is equal to $d^s{}_{max}$ - $d^s{}_{min}$[22], used to evaluate whether alkali ions and alkali atoms can be completely encapsulated by cyclocarbon and whether they can freely pass across the inner cyclocarbon. The value of SDP is larger than 0.0 Å in K@C_{14}, Na^+@C_{14}, and K^+@C_{14} complexes, indicating that C_{14} is unable to entirely adsorb K, Na^+, and K^+ into the ring. This suggests that C_{14} tends to obstruct the movement of these atoms and ions, preventing them from fully entering the ring structure. In contrast, C_{18} and C_{22} allow all the ions and atoms to reside within the same plane, exhibiting optimal host-guest interactions to be a suitable carbon-based host material for mitigating Na and K dendrite deposition without impeding Na^+ and K^+ ion diffusion.

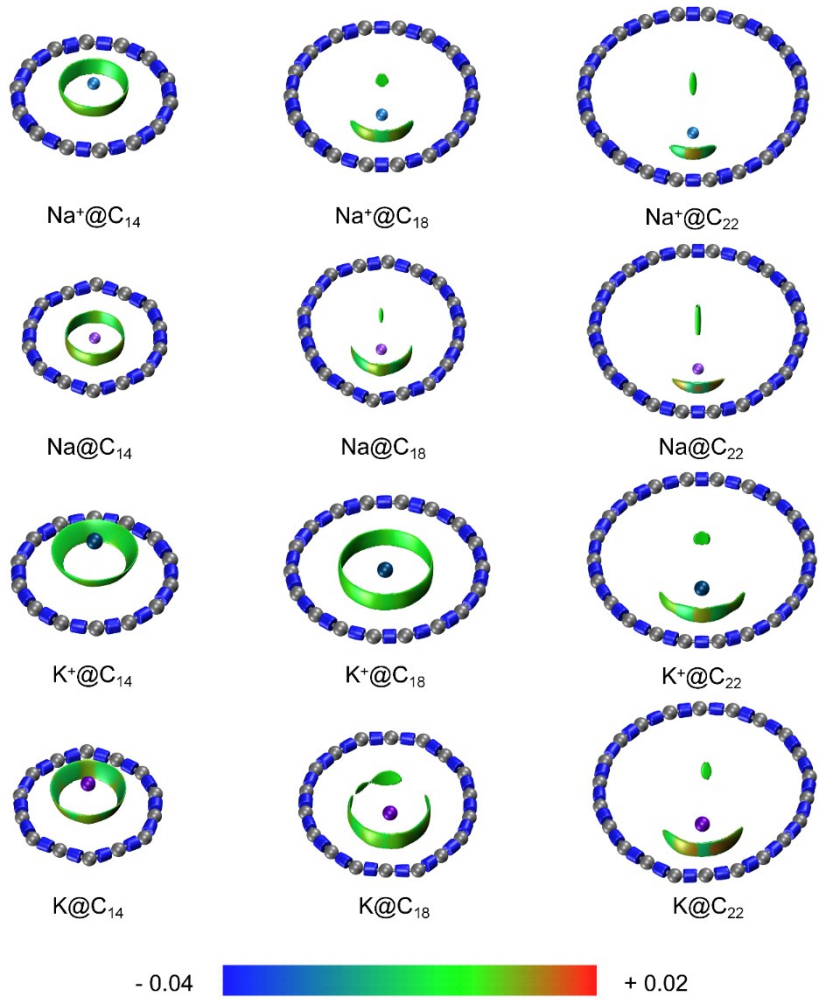

Figure S14. The interaction region indicator (IRI) maps of Na^+/Na and K^+/K interacted with C_{14}, C_{18} and C_{22}.

A weak interaction, characterized by the green region, is observed between cyclocarbon and Na^+/Na as well as K^+/K. This interaction is accompanied by a slight repulsion, indicated by the orange region.

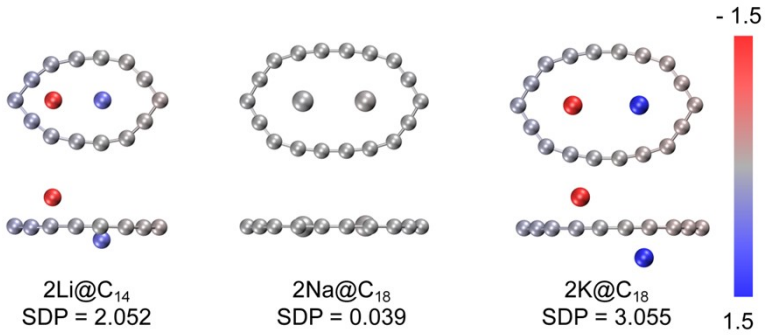

Figure S15. Geometries and the span of deviation from plane (SDP) for 2 Li atoms combined inside C_{14}, and 2 Na atoms or 2 K atoms combined inside C_{18}.

The value of SDP is larger than 0.0 Å in 2Li@C_{14}, 2Na@C_{18} and 2K@C_{18} complexes, suggesting C_{14} only can accommodate one Li atom, and C_{18} only can accommodate one Na atom or K atom.

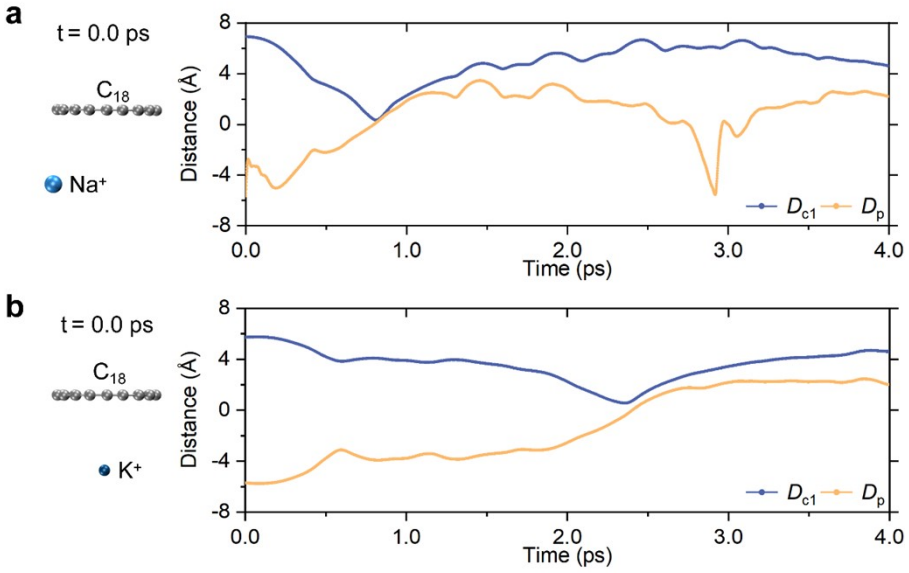

Figure S16. 4.0 ps trajectory of ab initio molecular dynamics simulations of outside Na^+ ion and K^+ ion across C_{18} at 300.00K, described by D_p (Blue) and D_{c1} (Yellow).

The level of ωB97XD/def-TZVP is adopted for *ab initio* molecular dynamics simulation. D_{c1} is the distance between the Li^+ ion or Li atom and the mass center. And D_p is the shortest perpendicular distance from the Li^+ ion or Li atom to the plane of C_{18}. **(a)**, The dynamical course of the Na^+ ion located 6.9 Å away from the center of C_{18} and -5.6 Å away from its plane. At 0.8 ps, both D_p and D_{c1} values approach 0.0 Å, indicating that the Na^+ ion entirely enters the C_{14} ring. Subsequently, these values deviate from 0.0 Å, indicating that the Na^+ ion can freely move out of the ring. **(b)**, The dynamical course of the K^+ ion located 5.7 Å away from the center of C_{18} and -5.7 Å away from its plane. At 2.4 ps, both D_p and D_{c1} values are close to 0.0 Å, indicating that the K^+ ion is entirely captured inside the C_{14} ring. These values then deviate from 0.0 Å, suggesting that the reversible freedom of K^+ ion diffusion would not be impeded by C_{18}.

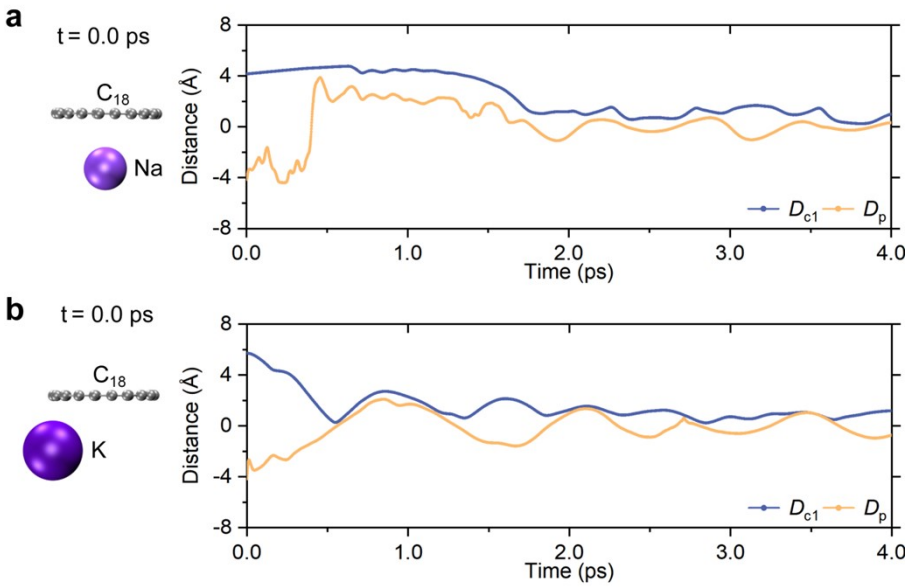

Figure S17. 4.0 ps trajectory of ab initio molecular dynamics simulations of outside Na atom and K atom, at different locations, interacting with C_{18}, described by D_p (Blue) and D_{c1} (Yellow).

The level of ωB97XD/def-TZVP is adopted for *ab initio* molecular dynamics simulation. D_{c1} is the distance between the Li^+ ion or Li atom and the mass center. And D_p is the shortest perpendicular distance from the Li^+ ion or Li atom to the plane of C_{18}. **(a)**, The dynamical course of the Na atom located 4.1 Å away from the center of C_{18} and -4.1 Å away from its plane. At 1.8 ps, both D_p and D_{c1} values approach 0.0 Å, indicating that the Na atom entirely enters the C_{14} ring. Subsequently, these values fluctuate around 0.0 Å, suggesting that the Na atom moves up and down within a limited area but cannot entirely escape the influence of C_{18}. **(b)**, The dynamical course of the K atom located 5.7 Å away from the center of C_{18} and -4.2 Å away from its plane. At 0.6 ps, both D_p and D_{c1} values are close to 0.0 Å, indicating that the K atom is entirely captured inside the C_{14} ring. Subsequently, these values fluctuate around this value, suggesting that the K atom moves up and down within the ring.

Table S5. The adsorption energy of Na^+/Na combined with conventional carbon-based materials in previous research.

Carbon-based materials	E_{adsNa^+} (kcal/mol)	E_{adsNa} (kcal/mol)	Reference
Graphene-$C_{94}H_{26}$	-41.3	-	[16]
Graphene-4×4	-	-16.4	[23]
Graphene-3×3	-	-16.6	[21]
Graphene-4×4	-	-14.3	[19]

Table S6. The adsorption energy of K^+/K combined with conventional carbon-based materials in previous research.

Carbon-based materials	E_{adsK^+} (kcal/mol)	E_{adsK} (kcal/mol)	Reference
Graphene-$C_{96}H_{26}$	-34.1	-	[16]
Graphene-3×3	-	-18.7	[21]
Graphene-4×4	-	-24.2	[19]

Table S7. The adsorption energy of Na^+/Na combined inside and outside C_{14}, C_{18} and C_{22}.

Cyclocarbon	Na^+		Na	
	E_{adsin} (kcal/mol)	E_{adsout} (kcal/mol)	E_{adsin} (kcal/mol)	E_{adsout} (kcal/mol)
C_{14}	-21.2	-17.8	-50.2	-31.1
C_{18}	-20.1	-16.5	-41.7	-30.5
C_{22}	-19.5	-17.2	-36.7	-29.3

Table S8. The adsorption energy of K^+/K combined inside and outside C_{14}, C_{18} and C_{22}.

Cyclocarbon	K^+		K	
	E_{adsin} (kcal/mol)	E_{adsout} (kcal/mol)	E_{adsin} (kcal/mol)	E_{adsout} (kcal/mol)
C_{14}	-13.6	-11.4	-56.3	-38.2
C_{18}	-16.1	-11.1	-54.8	-38.4
C_{22}	-14.3	-11.5	-48.8	-37.6

Table S9. The adsorption energy and the cell voltage of Na^+/Na combined with different carbon-based materials calculated in this work.

Carbon-based materials	E_{adsNa^+} (kcal/mol)	E_{adsNa} (kcal/mol)	ΔE_{tot} (kcal/mol)	V_{cell} (V)
C_{14}	-21.2	-50.2	29.0	-1.3
C_{18}	-20.1	-41.7	21.6	-0.9
C_{22}	-19.5	-36.7	17.2	-0.8
DV	-50.4	-56.4	5.0	-0.3
Graphene	-39.5	-15.2	-24.3	1.1
CNT(6,6)	-44.3	-36.8	-7.5	0.3

Table S10. The adsorption energy and the cell voltage of K^+/K combined with different carbon-based materials calculated in this work.

Carbon-based materials	E_{adsK^+} (kcal/mol)	E_{adsK} (kcal/mol)	ΔE_{tot} (kcal/mol)	V_{cell} (V)
C_{14}	-13.6	-56.3	42.7	-1.8
C_{18}	-16.1	-54.8	38.7	-1.7
C_{22}	-14.3	-48.8	34.5	-1.5
DV	-42.3	-68.4	26.1	-1.1
Graphene	-32.5	-26.5	- 6.0	0.3
CNT(6,6)	-39.8	-51.3	11.5	-0.5

Table S11. The length of the longest axis (*d*) and deform degree (*D*) for cyclocarbons interacted with Na^+/Na.

Cyclocarbon	*d* (Å)		*D* (%)	
	Na^+	Na	Na^+	Na
C_{14}	5.76	6.21	4.23	12.71
C_{18}	7.64	8.32	3.34	12.51
C_{22}	9.38	9.47	0.04	7.54

Table S12. The length of the longest axis (*d*) and deform degree (*D*) for cyclocarbons interacted with K^+/K.

Cyclocarbon	*d* (Å)		*D* (%)	
	K^+	K	K^+	K
C_{14}	5.76	6.15	3.45	6.11
C_{18}	7.39	7.95	3.92	4.96
C_{22}	9.33	9.69	3.43	7.40

Supplementary References.

(1) Aydinol, M. K.; Kohan, A. F.; Ceder, G.; Cho, K.; Joannopoulos, J. Ab initiostudy of lithium intercalation in metal oxides and metal dichalcogenides. *Phys. Rev. B* **1997**, *56* (3), 1354-1365.

(2) Ceder, G.; Aydinol, M. K.; Kohan, A. F. Application of first-principles calculations to the design of rechargeable Li-batteries. *Comput. Mater. Sci* **1997**, *8* (1-2), 161-169.

(3) Meng, Y. S.; Arroyo-de Dompablo, M. E. First principles computational materials design for energy storage materials in lithium ion batteries. *Energy Environ. Sci.* **2009**, *2* (6), 589-609.

(4) Julg, A.; Franois, P. Recherches sur la gomtrie de quelques hydrocarbures non-alternants: son influence sur les nergies de transition, une nouvelle dfinition de l'aromaticit. *Theor. Chim. Acta* **1967**, *8* (3), 249-259.

(5) Kresse, G.; Hafner, J. Ab initio Hellmann-Feynman molecular dynamics for liquid metals. *J. Non-Cryst. Solids* **1993**, *156-158*, 956-960.

(6) Kresse, G.; Hafner, J. Ab initio molecular-dynamics simulation of the liquid-metal-amorphous-semiconductor transition in germanium. *Phys. Rev* **1994**, *49* (20), 14251-14269.

(7) Kresse, G.; Furthmüller, J. Efficiency of ab-initio total energy calculations for metals and semiconductors using a plane-wave basis set. *Comput. Mater. Sci* **1996**, *6* (1), 15-50.

(8) Kresse, G.; Furthmuller, J. Efficient iterative schemes for ab initio total-energy calculations using a plane-wave basis set. *Phys. Rev* **1996**, *54* (16), 11169-11186.

(9) Kresse, G.; Joubert, D. From ultrasoft pseudopotentials to the projector augmented-wave method. *Phys. Rev. B* **1999**, *59* (3), 1758-1775.

(10) Perdew, J. P.; Burke, K.; Ernzerhof, M. Generalized Gradient Approximation Made Simple. *Phys. Rev. Lett.* **1996**, *77* (18), 3865-3868.

(11) Grimme, S.; Antony, J.; Ehrlich, S.; Krieg, H. A consistent and accurate ab initio parametrization of density functional dispersion correction (DFT-D) for the 94 elements H-Pu. *J. Chem. Phys.* **2010**, *132* (15), 154104.

(12) Parrish, R. M.; Burns, L. A.; Smith, D. G. A.; Simmonett, A. C.; DePrince, A. E., 3rd; Hohenstein, E. G.; Bozkaya, U.; Sokolov, A. Y.; Di Remigio, R.; Richard, R. M.; Gonthier, J. F.; James, A. M.; McAlexander, H. R.; Kumar, A.; Saitow, M.; Wang, X.; Pritchard, B. P.; Verma, P.; Schaefer, H. F., 3rd; Patkowski, K.; King, R. A.; Valeev, E. F.; Evangelista, F. A.; Turney, J. M.; Crawford, T. D.; Sherrill, C. D. Psi4 1.1: An Open-Source Electronic Structure Program Emphasizing Automation, Advanced Libraries, and Interoperability. *J. Chem. Theory Comput.* **2017**, *13* (7), 3185-3197.

(13) Udomvech, A.; Kerdcharoen, T.; Osotchan, T. First principles study of Li and Li+ adsorbed on carbon nanotube: Variation of tubule diameter and length. *Chem. Phys. Lett.* **2005**, *406* (1-3), 161-166.

(14) Gao, S.; Shi, G.; Fang, H. Impact of cation-pi interactions on the cell voltage of carbon nanotube-based Li batteries. *Nanoscale* **2016**, *8* (3), 1451-1455.

(15) Shanmugam, S.; Nachimuthu, S.; Subramaniam, V. The effect of edge termination on Li+ ion adsorption of pristine and defected graphene sheets. *J. Mater. Sci.* **2020**, *55* (14), 5920-5937.

(16) Sangavi, S.; Santhanamoorthi, N.; Vijayakumar, S. Density functional theory study on the adsorption of alkali metal ions with pristine and defected graphene sheet. *Mol. Phys.* **2018**, *117* (4), 462-473.

(17) Zheng, J.; Ren, Z.; Guo, P.; Fang, L.; Fan, J. Diffusion of Li+ ion on graphene: A DFT study. *Appl. Surf. Sci.* **2011**, *258* (5), 1651-1655.

(18) Kheirabadi, N.; Shafiekhani, A. Graphene/Li-ion battery. *J. Appl. Phys.* **2012**, *112* (12).

(19) Olsson, E.; Chai, G.; Dove, M.; Cai, Q. Adsorption and migration of alkali metals (Li, Na, and K) on

pristine and defective graphene surfaces. *Nanoscale* **2019**, *11* (12), 5274-5284.
(20) Wu, D. H.; Li, Y. F.; Zhou, Z. First-principles studies on doped graphene as anode materials in lithium-ion batteries. *Theor. Chem. Acc.* **2011**, *130* (2-3), 209-213.
(21) Nakada, K.; Ishii, A. Migration of adatom adsorption on graphene using DFT calculation. *Solid State Commun.* **2011**, *151* (1), 13-16.
(22) Lu, T. Simple, reliable, and universal metrics of molecular planarity. *J. Mol. Model.* **2021**, *27* (9).
(23) Yao, L.-H.; Cao, W.-Q.; Cao, M.-S. Doping effect on the adsorption of Na atom onto graphenes. *Curr. Appl Phys.* **2016**, *16* (5), 574-580.